Absolute CH Radical Concentrations in Rich Low-Pressure Methane−Oxygen−Argon Flames via Cavity Ringdown Spectroscopy of the $A^2\Delta-X^2\Pi$ Transition

John W. Thoman, Jr.

Chemistry Department, Williams College, 47 Lab Campus Drive, Williamstown, Massachusetts 01267

Andrew McIlroy*

Combustion Research Facility, Sandia National Laboratories, MS 9055, P.O. Box 969, Livermore, California 94551-0969

Received: January 12, 2000; In Final Form: March 27, 2000

We measure absolute methylidyne (CH) radical concentrations in a series of rich 31.0 Torr (4.13 kPa) methane−oxygen−argon flames using cavity ringdown spectroscopy. Probing via the CH $A^2\Delta-X^2\Pi$ transition near 430 nm gives a sensitivity of 3×10^9 cm^{-3} for our experimental conditions, yielding a signal-to-noise ratio greater than 1000 for the strongest transitions observed. We measure profiles of CH mole fraction as a function of height above a flat-flame burner for rich flames with equivalence ratios of 1.0, 1.2, 1.4, and 1.6. These flames are modeled using the following mechanisms: (1) the GRI Mech 2.11, (2) a mechanism by Prada and Miller, (3) a modified GRI 2.11 mechanism, which employs a more realistic increased CH + O_2 rate coefficient, and (4) the new GRI Mech 3.0. Generally good agreement between the models and the data is found, with the GRI 3.0 and modified 2.11 mechanisms best reproducing the data. The greatest discrepancies are observed at the richest stoichiometry, where all of the models predict a wider CH profile shifted further from the burner than experimentally observed.

Introduction

The methylidyne (CH) radical is a widely-studied intermediate of importance in many gas-phase hydrocarbon chemical processes, including combustion[1] and production of synthetic diamond.[2] Attention has been focused on the detection of CH in flames because of the importance of the CH + N_2 reaction in prompt NO formation.[1] Although in general only a small fraction of hydrocarbon oxidation proceeds through a pathway that includes CH radicals,[3] CH plays a key role in the formation of both NO_x and soot pollutants. The CH radical also participates in NO_x reburning.[1] Quantitative measurements of CH concentrations in flames assist in optimizing chemical kinetic models of combustion.[4] Though the HCO radical has recently been shown to be a better indicator of the heat release in a flame,[5] CH radical concentration is often used as an indicator of the flame front in combustion of hydrocarbons.[6] Because CH appears in only a narrow region of the flame and has convenient optical transitions, planar laser-induced fluorescence (pLIF) or emission images produce compelling pictures of the flame front. The challenge of fluorescence-based techniques is to account for quenching processes and for detection efficiencies in order to convert the signals to number densities.

The absolute concentration of CH in hydrocarbon flames is low, on the order of 10 ppm, or approximately 3 orders of magnitude lower than the ubiquitous OH radical in the simple flames considered here. Thus, probe techniques must be sensitive, as well as selective. Numerous methods have been used to detect CH radicals. CH has been detected in flames, plasmas, and jets by Fourier transform absorption spectroscopy,[7] linear laser-induced fluorescence (LIF) calibrated with Raman or Rayleigh scattering,[8] saturated LIF,[9] picosecond time-resolved LIF,[10] degenerate four-wave mixing (DFWM),[11,12] two-color laser-induced grating spectroscopy (TC-LIGS),[13−15] wavelength-modulation diode laser absorption spectroscopy,[16] and resonance-enhanced coherent anti-Stokes Raman spectroscopy (RE-CARS).[17] Emission spectroscopy of CH has also been used to monitor flames, though it is really a measure of the excited ($A^2\Delta$) state population, rather than the ground ($X^2\Pi$) state population probed by the other methods mentioned above.

Each of these methods has advantages and disadvantages. Fluorescence-based techniques have dominated the CH diagnostic literature; however, they must overcome the difficulties related to quenching effects and detection efficiencies to produce quantitative results. In principle, absorption-based methods could overcome these problems, but historically, low sensitivity and poor spatial resolution have limited the utility of these methods. Single-pass absorption is generally not sufficient for the detection of CH radicals, and thus multipass absorption is required for a Beer's law detection scheme. Traditional multipass cells, such as a White or Herriott cell, probe a large volume and thus lack spatial sensitivity. Additionally, traditional multipass cells may be limited in the path length obtainable. Our choice of cavity ringdown spectroscopy largely eliminates these difficulties. Cavity ringdown is a line-of-sight technique that, when properly aligned, retains spatial resolution along a single line within the sample volume. With the appropriate high-reflectivity mirrors, effective Beer's law path lengths in excess of a kilometer are readily obtained.

Here, we report cavity ringdown measurements of the $A^2\Delta-X^2\Pi$ transition near 430 nm for CH radicals in low-pressure flat flames, and compare the results to model calculations. Cavity

* Corresponding author. Phone: (925) 294-3054. Fax: (925) 294−2276. E-mail: amcilr@sandia.gov.

10.1021/jp0001687 CCC: $19.00
Published on Web 05/03/2000

ringdown (or cavity ringdown laser absorption spectroscopy, as it is also known) was first demonstrated in a chemical application by O'Keefe and Deacon,[18] who detected molecular oxygen in the doubly forbidden b−X electronic transition. Since that time, there has been a veritable explosion in the application and extension of the technique. A review by Scherer et al.[19] and an American Chemical Society Symposium Series book[20] highlight the extensions and applications of the technique. Cavity ringdown is well suited to detection of trace species such as OH,[21,22] singlet CH_2,[23] CH_3,[24] and HCO[25] in both low-pressure and atmospheric-pressure flames. Thoman et al.[26] have used cavity ringdown spectroscopy on the CH $A^2\Delta-X^2\Pi$ transition to measure rotational and vibrational temperatures of CH in an air−acetylene slot burner. Other groups have employed the $C^2\Sigma^+-X^2\Pi$ band near 315 nm for cavity ringdown spectroscopy of CH in low-pressure flat flames[27] and atmospheric-pressure diffusion flames.[28] The CH $C^2\Sigma^+-X^2\Pi$ transition is favorable because it overlaps the OH $A^2\Sigma^+-X^2\Pi$ transition, so that both radicals can be detected without changing optical systems. Derzy et al.[27] suggest that the CH sensitivity should be greater when using the $C^2\Sigma^+-X^2\Pi$ transition because its absorption cross section is 30% larger than the $A^2\Delta-X^2\Pi$ transition, albeit with a simultaneous increase in the uncertainty of the cross section. In this paper, we show that the CH sensitivity is greater using the $A^2\Delta-X^2\Pi$ transition, largely because lower background losses are achieved. The background losses are primarily due to mirror losses, but some additional loss is attributable to scattering from particulates in the flame. Indeed, Vander Wal and Ticich[29] have used a calibrated cavity ringdown technique to quantify soot in flames.

Measurements of CH have been used as targets in the development of chemical kinetic models of hydrocarbon combustion, such as GRI Mech.[30,4] Derzy et al.[27] found that their CH ringdown measurements agreed reasonably well with model results for low-pressure, near-stoichiometric methane−air flames. For each flame, however, they found that the experimental results were ∼20% lower than the model predictions. They comment that the discrepancy could be due to either difficulties in the model or nonideality of the flame. Since Derzy et al. do not report extensive error analyses, one might also include experimental uncertainty as a cause of discrepancy between the experimental and model results. Woiki et al.[31] used diode laser absorption to measure CH radical concentrations behind well-characterized shock waves and compared their observations to the calculations using GRI Mech 2.11. In shocks that included NO, they found CH concentrations in reasonable agreement with the GRI Mech model predictions. With shocks that included methane and oxygen but no nitrogen compounds, however, Woiki et al.[31] found CH concentrations approximately a factor of 2 below those predicted by GRI Mech 2.11 calculations. They suggest that the $CH + O_2$ reaction rate coefficient, which has been measured at temperatures above 2000 K,[32,33] is 3 times higher at flame conditions than the rate included in GRI Mech 2.11. The recent update of GRI Mech, version 3.0, includes this modified rate as well as other significant changes in the CH chemistry.[4] When NO is included, the CH removal rate via $CH + O_2$ is overwhelmed by loss via the CH + NO reaction. In this paper, we compare our experimental results with chemical kinetic model calculations and demonstrate that the observations support the incorporation of a larger $CH + O_2$ rate coefficient at flame temperatures.

Experimental Section

Flames. The low-pressure flame and optical diagnostics systems used in the present work are described in earlier papers on singlet methylene[23] and formyl radicals.[34] The flames studied in these previous experiments are used in the present work, but a probe laser with narrower bandwidth is employed. Well-characterized[34] rich methane−oxygen−argon flames with equivalence ratios, ϕ, of 1.0, 1.2, 1.4, and 1.6 are studied on a 6-cm-diameter McKenna burner in a chamber maintained at a pressure of 31.0 Torr (4.13 kPa). Argon is added as a diluent to increase the lift-off of the flame front from the burner and to achieve visually flat flames. Argon is also used in a shroud flow to help contain the flame and in a mirror-purge flow to help keep the ringdown mirrors clean. Mass flow controllers, calibrated with a NIST traceable floating piston and stopwatch, control flows of commercially available argon, oxygen, and methane. Flame temperature profiles are obtained from previous OH LIF measurements of the same flames.[23]

Optical. For nanosecond-pulsed cavity ringdown spectroscopy on the Q and R branches of the CH $A^2\Delta-X^2\Pi$ transition near 430 nm, we use two laser systems. The first system consists of a dye laser with stilbene-3 dye and a nominal 0.15 cm^{-1} spectral bandwidth and 2.5 ns temporal bandwidth pumped by the third harmonic of a Nd:YAG laser running at repetition rates up to 100 Hz. For measuring absolute concentrations, we use a 10 Hz, 5 ns temporal pulse width, 0.02 cm^{-1} spectral bandwidth, Nd:YAG-pumped optical parametric oscillator/optical parametric amplifier (OPO/OPA) laser system. Two 3:1 telescopes, each formed by two convex lenses and a 75 μm stainless steel pinhole, are used to spatially filter and to reduce the diameter of the laser pulses for coupling to the ringdown cavity. Two 6 m radius mirrors, 99.99+% reflectivity at 430 nm, are used to form a 72.5 cm cavity. Typically, 10 μJ per pulse is incident on the back face of the entrance ringdown mirror. The ringdown signal is collected with a fast photomultiplier tube, amplified with a 300 MHz video amplifier, and collected with an 8-bit vertical resolution digital oscilloscope. The laser, burner translation, and data acquisition system are computer controlled. In a typical absorption spectrum, 20 decay curves at each laser frequency are co-added and then fit to a decay coefficient. In profiling the CH radical concentration as a function of height above the burner, 100 shots are averaged at each height, and the burner is stepped in 0.025 cm intervals, approximately one-half the laser beam size. Profiles are recorded with the laser tuned both to the peak of a rovibronic transition and also to a nonresonant background. Total cavity losses are converted to loss due to CH absorption by subtraction of the nonresonant background signals. This procedure effectively removes the contributions due to scattering by particulates and the reflectivity of the mirrors.

CH radical ringdown signals are converted to CH number densities taking into account the finite laser bandwidth, the Gaussian line shape factor, the Boltzmann fraction using the previously measured temperature profiles,[23] and the Einstein A coefficients from Luque and Crosley[35] as tabulated in the LIFBASE program.[36] In calculating mole fractions, we assume Gaussian line shapes for both the laser spectral profile and the molecular line width. Rotational and vibrational temperatures are calculated using our CH ringdown signals, line-strength factors tabulated by Beenaker et al.,[37] rotational energies calculated according to Baas and Beenakker,[38] Franck−Condon factors reported by Garland and Crosley,[39] and the assumption of a Boltzmann internal energy distribution.

To obtain good spatial resolution in the profiles of CH number density as a function of distance above the surface of the burner, we monitor the spatial profile of the ringdown laser beam after it exits the ringdown cavity with a gated, intensified CCD

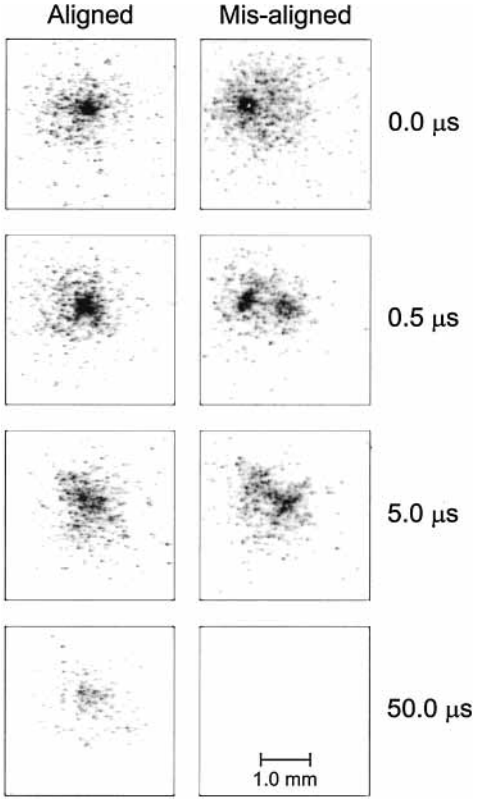

Figure 1. Images of the ringdown laser beam after it has exited the ringdown cavity, recorded with a 20 ns gate width on an intensified CCD camera. Delay times of 0, 0.42, 5, and 50 μs are shown for an aligned (left images) and deliberately misaligned cavity. Two spots appear in the misaligned case, whereas a single spot is present when the ringdown cavity is well aligned.

camera system. Using a 20 ns gate, we confirm that the beam diameter (fwhm) is less that 0.5 mm, and that the ringdown beam remains in the same position for the ~20 μs analysis time of the ringdown signal. If the ringdown cavity is slightly misaligned, then two spots are visible in the image of the beam and more beam walk is observed during the ringdown, as shown in Figure 1.

Calibration of the height above the burner is accomplished by translating the burner until it eclipses the ringdown beam, thus defining the "zero" height. To check the burner height calibration, we place a 2 mm wide spectrometer slit assembly on the burner (in the absence of a flame) and translate the burner so that the ringdown beam passes through the slits and is eclipsed sequentially on the top and the bottom. Calibration checks of this sort suggest that the burner height uncertainty is ±0.5 mm, or 2 burner steps, for our typical experimental conditions.

To check the uniformity of the flame in two dimensions, we record pLIF images of the CH radicals. For the pLIF experiments, ~1 mJ of laser light from the OPO/OPA system is shaped into a ~1 cm high, ~1 mm thick sheet using two cylindrical lenses. This light is used to excite the CH $A^2\Delta-X^2\Pi$ (0,0) R_{2e}-(7.5) transition, and fluorescence from the (0,0) transition is imaged using a 430 ± 5 nm band-pass filter and a 60 mm macro lens. The camera system used to align the ringdown cavity is also used in the pLIF experiments. For the pLIF experiments, a 12 ns gate is set just after the laser pulse to avoid scattered light and to minimize the effects of quenching. The pLIF laser sheet is rotated 45° from the CRDS laser axis, but the flame is cylindrically symmetric, so the interpretation is the same as if the CRDS and pLIF laser probed the same region of the flame.

TABLE 1: Flame Conditions: Mole Fractions and Total Flow Rates[a]

ϕ	$X(CH_4)$	$X(O_2)$	X(Ar)	flow rate (g/cm^2)
1.0	0.107	0.215	0.678	0.000 62
1.2	0.137	0.229	0.633	0.007 29
1.4	0.168	0.241	0.591	0.006 78
1.6	0.225	0.275	0.500	0.005 66

[a] P = 31.0 Torr (4.13 kPa) for all flames.

Modeling

Predictions of CH radical number densities are calculated using the CHEMKIN II software package[40−43] for premixed 1-D laminar flames. We use four different chemical mechanisms: Prada-Miller,[44] GRI Mech 2.11[30] and 3.0,[4] and GRI Mech 2.11 with an increased value of the CH + O_2 rate coefficient as described below. All calculations are run in the fixed temperature profile mode with temperatures previously obtained from Boltzmann plots of OH LIF signals, corrected for probe laser intensity fluctuation, probe laser absorption, and J-dependent quenching, as inputs to the model calculations.[23]

Results

CH Ringdown Results. Cavity ringdown spectra of the Q and R branches of the CH $A^2\Delta-X^2\Pi$ electronic transition are obtained in low-pressure methane−oxygen flames with equivalence ratios ranging from 1.0 to 1.6. The equivalence ratio is taken as $2[CH_4]/[O_2]$, and the flame conditions are listed in Table 1. Between 426 and 431.5 nm (23 180−23 840 cm^{-1}) we observe more than 300 CH rovibronic transitions. Figure 2a, shows the flat, quiet baseline achievable in a low-pressure flame and the overall decrease in signal intensity with rotational quantum number, N'', in a portion of the R-branch. The (1,1) hot band transitions are also readily apparent, with signal strengths on the order of 15% of the neighboring (0,0) transitions. Essentially all observed lines are assigned using the tables in Gero,[45] the graphical output of the LIFBASE program,[36] and the high-precision wavelength measurements of Bernath et al.[7] Isotopic transitions are assigned using the tables in Zachwieja.[46] Figure 2b shows the (1,1) and (2,2) hot bands in addition to the (0,0) bands at 0.6 cm above the burner in ϕ = 1.4 flame. For the stronger CH lines, such as the N'' = 8 lines in the R-branch of the $A^2\Delta-X^2\Pi$ transition near 23 460 cm^{-1} (Figure 2), the signal is ~2000 ppm/pass, the baseline noise is ~2 ppm/pass, and the signal-to-noise (S/N) ratio is ~1000 for 20 shot averaging. The Nd:YAG-pumped dye laser is usually run at an 80 Hz repetition rate, which corresponds to 0.25 s per laser step. This S/N ratio suggests a detection limit of approximately 3×10^9 cm^{-1} for CH radicals at 2000 K, which corresponds to 5×10^7 molecule^{-3}/quantum state or about 2 ppm/pass.

The sensitivity and S/N ratio is further demonstrated in Figure 2b, where the vertical scale has been substantially expanded. Transitions resulting from the naturally occurring (1.11%)[47] ^{13}CH are clearly visible when they do not overlap a ^{12}CH line. Indeed, hot-band isotopic transitions, such as the ^{13}CH $A^2\Delta-X^2\Pi$ (1,1) R_{2e}(7.5) line at 23 444.74 cm^{-1}, are distinguishable at only a few ppm/pass. With a natural abundance of only 0.015% for deuterium, the strongest CD $A^2\Delta-X^2\Pi$ (0,0) transitions would be less than 0.5 ppm/pass, which is below our detection limit. Substantially more signal averaging would be needed to detect CD radicals in natural abundance.

The evacuated cavity has a ringdown time greater than 60 μs. For our 72.5 cm long cavity, this corresponds to a mirror

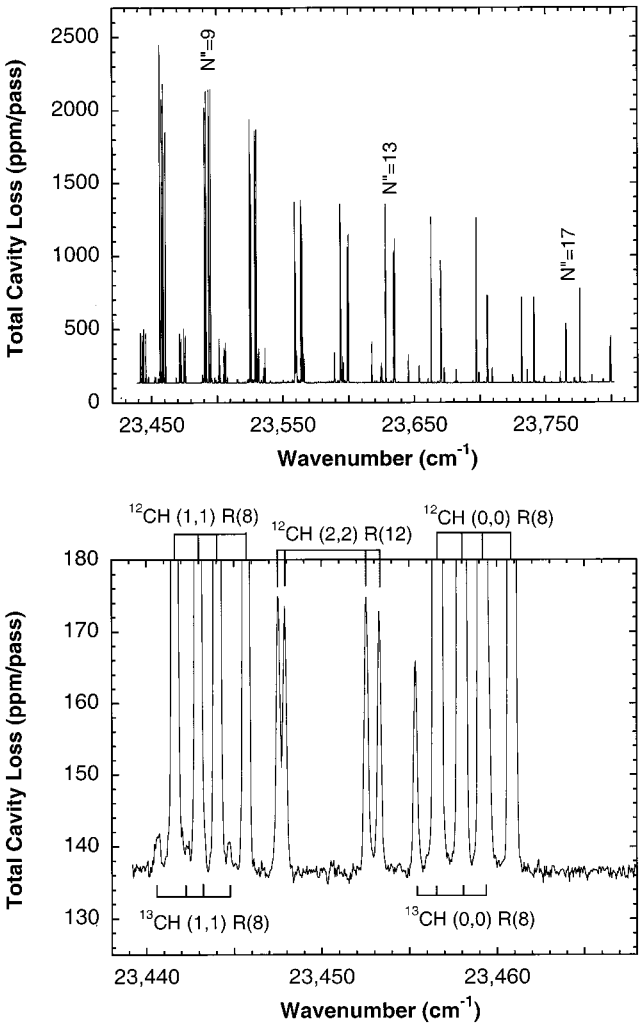

Figure 2. CH $A^2\Delta-X^2\Pi$ cavity ringdown spectrum recorded at 0.6 cm above a 6.0 cm McKenna burner in a $\phi = 1.4$ $CH_4/O_2/Ar$ flame with a 0.15 cm^{-1} dye laser. (a, top) R-branch region from $N'' = 8$ to $N'' = 18$. The spectrum is recorded by averaging 20 laser shots at each 0.001 nm step of the dye laser. For each N'' state, there are four transitions, R_{1e}, R_{1f}, R_{2e}, and R_{2f}, due to lambda doubling and spin−orbit splitting. (b, bottom) Detail showing the baseline noise level in the (0,0) $N'' = 8$, (1,1) $N'' = 8$, and (2,2) $N'' = 12$ regions of the spectrum. Naturally abundant ^{13}CH isotope lines and ^{13}CH isotope hot bands are also visible.

reflectivity of 99.995+% and a loss of about 40 ppm/pass. When a typical flame is probed off-resonance near the position of maximum CH concentration, the off-resonant ringdown time drops to 20 μs, or about 125 ppm/pass. The additional loss may be due to thermal gradient induced beam steering and/or scattering by particulates in the flame. There is a small increase in off-resonant loss with increasing flame stoichiometry, suggesting that particulate scattering may play a significant role. We note that cavity ringdown has been used to detect atmospheric particulates[48] and to detect soot in low-pressure flames.[29] The maximum in the nonresonant background loss occurs at a height above the burner that is very close to the height of the maximum CH cavity ringdown signal, which is also very close to the maximum CH number density.

Careful examination of Figure 2b reveals some anomalous variations of intensity with J. The ~30 ppm/pass peak intensity of the ^{13}CH (0,0) $R_{1e}(8.5)$ transition is more than the ~25 ppm/pass expected given the ~2300 ppm/pass peak intensity of the ^{12}CH (0,0) $R_{1e}(8.5)$ transition and the flame temperature. The primary reason for this is that the dye laser spectral bandwidth

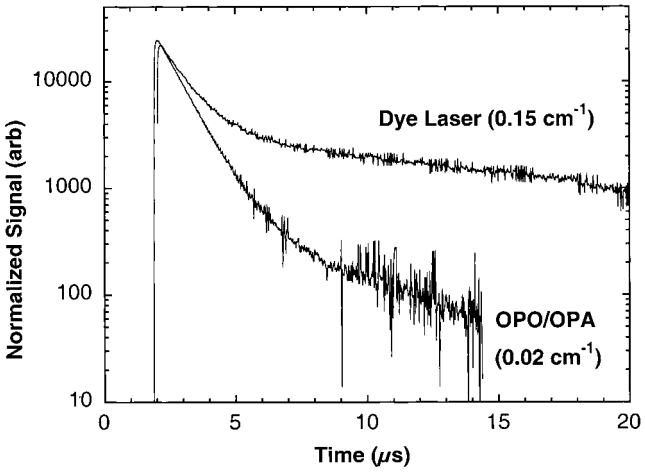

Figure 3. Cavity ringdown signals for a 0.15 cm^{-1} dye and 0.02 cm^{-1} OPO/OPA laser system exciting at the peak of the CH $A^2\Delta-X^2\Pi$ (0,0) $R_{2e}(7.5)$ transition in a 31 Torr, $\phi = 1.2$ $CH_4/O_2/Ar$ flame.

used in Figure 2, 0.15 cm^{-1}, is comparable to the Doppler line width, 0.20 cm^{-1}, for CH at 2000 K at this transition frequency. Several papers, including those by Zalicki and Zare,[49] Romanini and Lehmann,[50] and Hodges, Looney and van Zee,[51] have highlighted the problems that arise when the laser line width is of the same order as the molecular line width. These authors have also quantified the operating conditions needed to extract reliable signal intensities. To obtain quantitative CH concentrations, we use a second laser system, an OPO/OPA, with a 0.02 cm^{-1} spectral bandwidth. The OPO/OPA spectral bandwidth is an order of magnitude narrower than the CH molecular line width for the flames used. With the narrow-bandwidth laser, we obtain single-exponential decay ringdown curves as shown in Figure 3. In contrast, when the 0.15 cm^{-1} dye laser excites the "edge" as well as the "peak" of a transition, non-single-exponential decays are seen. To extract approximate ringdown signals from these multiexponential decays, we fit only the very early ringdown time to a single-exponential decay. However, this method is clearly inappropriate for quantitative measurements of CH concentration. With the 0.02 cm^{-1} OPO/OPA laser, we typically fit single-exponential decays using 10−90% of the ringdown curve amplitude to obtain the total cavity loss per pass. This region of the ringdown curve is well fit by a single-exponential decay. The ppm/pass signals obtained with the 0.02 cm^{-1} OPO/OPA laser are roughly 50% larger than those obtained with the 0.15 cm^{-1} dye laser, again highlighting the importance of laser line width. The peak shapes of isolated CH rotational lines obtained using the 0.02 cm^{-1} OPO/OPA laser (Figure 4) are fit well by a Voigt line shape with a fwhm of 0.196 cm^{-1}. The Gaussian component fwhm is 0.182 cm^{-1}, and the Lorentzian component is 0.027 cm^{-1}. Thus these lines can be well approximated by a Gaussian line shape for the purpose of extracting CH concentrations from peak absorption intensities.

Using CH cavity ringdown measurements, we measure temperatures using a Boltzmann plot such as Figure 5. The temperatures thus measured are ~10% above those measured with OH LIF, but within the experimental uncertainties. For all cases we considered, the CH rotational temperatures in $v'' = 0$ and $v'' = 1$ are the same, and the vibrational temperature is the same as the rotational temperature within the experimental uncertainty of ±200 K for vibrational temperatures. It is possible that the CH vibrational temperature is larger than the rotational temperature for certain regions of the flame, but we did not investigate this possibility. Because OH is present in measurable concentrations over a broad range of heights above the burner,

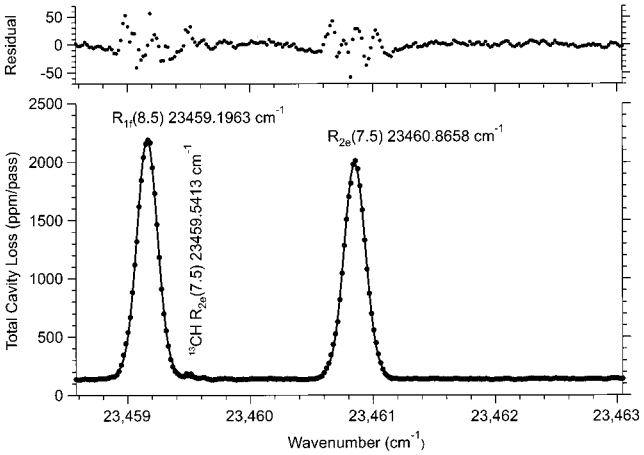

Figure 4. CH $A^2\Delta-X^2\Pi$ (0,0) $R_{2e}(7.5)$ and $R_{1f}(8.5)$ rotational transitions probed 0.65 cm above the burner in a 31 Torr, $\phi = 1.2$ $CH_4/O_2/Ar$ flame fit with Voigt line shapes of 0.20 cm^{-1} fwhm. The Doppler width for these transitions is 0.208 cm^{-1} (fwhm) at 2000 K. At the top of the plot, the residuals of the fit are shown with an expanded vertical scale. The spectrum is recorded by averaging 10 laser shots at each 0.0003 nm step of the OPO.

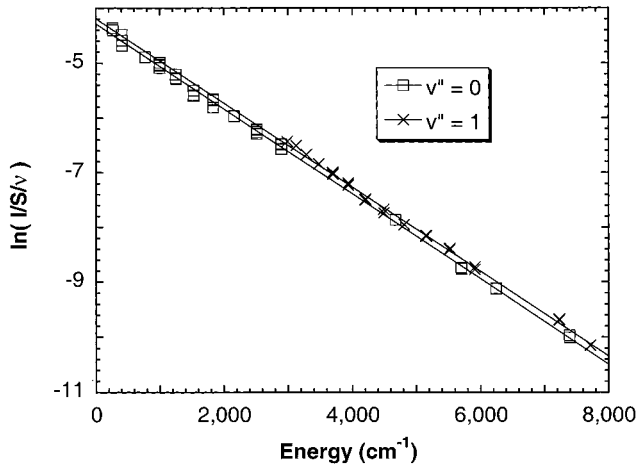

Figure 5. Boltzmann plot for determining the CH rotational temperature transitions probed 0.5 cm above the burner in a 31 Torr, $\phi = 1.0$ $CH_4/O_2/Ar$ flame. For $v'' = 0$, $T_{rot} = 1854 \pm 30$ K while for $v'' = 1$, $T_{rot} = 1872 \pm 30$ K. Based on the intensities used in making this plot, we calculate $T_{vib} = 2050 \pm 200$ K. From previous OH LIF measurements, $T = 1780$ K.

and because with LIF we can measure concentrations closer to the burner surface than we can with cavity ringdown, we use flame temperature profiles in the model calculations derived from OH LIF measurements.[23]

Because cavity ringdown (like all absorption-based techniques) is a line-of-sight technique, our calculation of radical number density assumes a top-hat profile of CH radicals above the surface of the burner. We use the 6.00 cm burner diameter as the path length in our calculations and assume that the flame is uniform along the line. To test these assumptions, we collect pLIF images of CH above the surface of the burner. Distances in the images are calibrated by taking a picture of a ruler with the same camera and focal plane as used for flame imaging. Figure 6 shows a contour plot of CH pLIF signal in a $\phi = 1.2$ flame along with a profile generated from a slice parallel to the burner surface, through the maximum of the CH concentration. The profile shows how the CH number density varies along that line. We have not corrected the CH LIF images for temperature or quenching variations along the profile. For the range of temperatures expected, the $N'' = 8$ lines are relatively

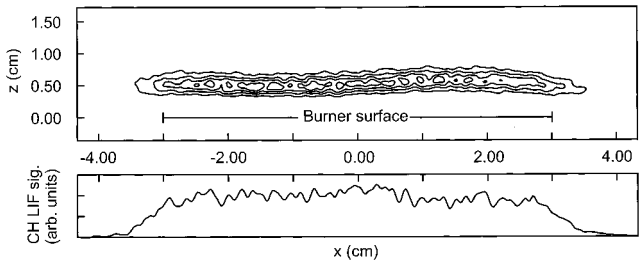

Figure 6. Contour map of a planar laser-induced fluorescence image of CH, exciting $A^2\Delta-X^2\Pi$ (0,0) $R_{2e}(7.5)$ in a 31 Torr, $\phi = 1.2$ $CH_4/O_2/Ar$ flame. The image is the sum of signals from 50 laser shots minus a 50 shot background image taken with the probe laser blocked. The gate of the intensified CCD camera is set to collect fluorescence between 20 and 32 ns after the start of the laser pulse. Resonance fluorescence is imaged through a 430 ± 5 nm band-pass filter. The data are 9-point smoothed prior to contouring and plotting. The *x*-axis zero is at the burner surface, and the extent of the burner surface is noted on the figure. The lower panel displays a cut through the data at the maximum intensity. Note that <10% of the fluorescence intensity appears outside the 6 cm diameter burner width and that the CH profile is relatively flat across the burner.

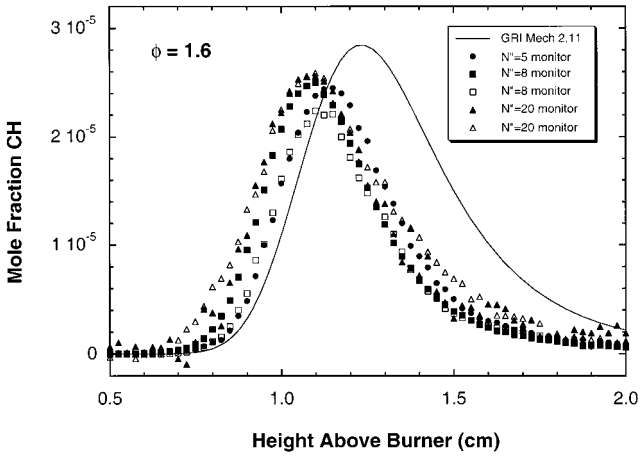

Figure 7. Reproducibility of the CH mole fraction profile in a 31.0 Torr, $\phi = 1.6$ $CH_4/O_2/Ar$ flame probed on three different rotational transitions on four different days. The results of a model calculation using GRI Mech 2.11 are shown for comparison.

insensitive to Boltzmann factor corrections. We measured LIF images for both $N'' = 8$ and $N'' = 5$ to check for any temperature variations and found no apparent variation in the relative signal stengths. Integration of the pLIF signal profile within the 6 cm burner dimension reveals that >90% of the signal is generated in this region. Thus, our assumption of a 6 cm path length for ringdown data analysis is reasonable, although generally a lower limit.

To test the reproducibility of our measurements and to gauge the extent of systematic errors, we repeatedly profile the same flame using different rotational transitions and calculate the mole fraction profile, as shown in Figure 7. Results from experiments in $\phi = 1.6$ flames on four different days using three different rotational lines agree within 12% for peak mole fraction and within 8% for peak height above burner. The $\phi = 1.6$ flame was chosen because, of the flames studied, it is most sensitive to small changes in the gas flow rates. The agreement of CH mole fractions when using rotational lines with some of the largest ($N'' = 5$) and smallest ($N'' = 20$) ringdown signals in ppm/pass lends confidence to both our spectroscopic assignments and our data analyses. Data taken with our 0.15 cm^{-1} dye laser, instead of the 0.02 cm^{-1} OPO, show large and systematic variation of calculated mole fraction with N''. These

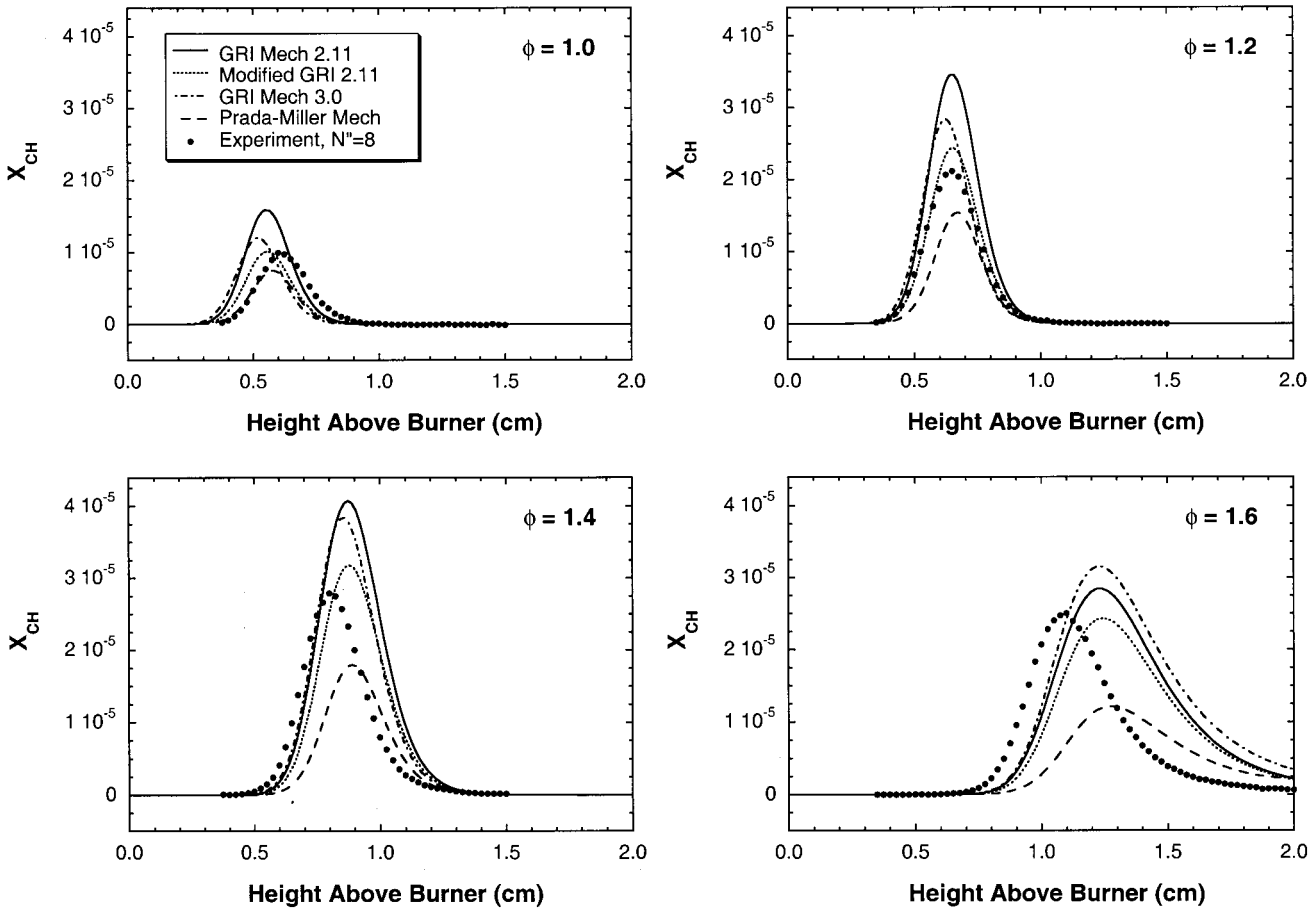

Figure 8. CH profiles for 31 Torr $CH_4/O_2/Ar$ flames with four different equivalence ratios compared with chemical kinetics model results. Four different chemical mechanisms are used in the modeling: Prada-Miller, GRI Mech 2.11, GRI Mech 3.0, and GRI Mech 2.11 modified to include a 3× faster rate coefficient for the CH + O_2 reaction as described in the text.

variations highlight the importance of choosing a laser bandwidth commensurate with the transition spectral width.

Experimentally measured number densities for flames with equivalence ratios $\phi = 1.0$, 1.2, 1.4, and 1.6 are compared with the results of model calculations in Figure 8. In each case, the peak experimental mole fractions are smaller than the GRI Mech 2.11[30] model predictions and larger than the Prada−Miller[44] mechanism model predictions. The models that most closely reproduce the peak experimental values are a modified GRI Mech 2.11 mechanism and the GRI Mech 3.0 mechanism.[4] The modified GRI Mech 2.11 mechanism includes a 3 times larger rate coefficient for the CH + O_2 reaction (as described in the Discussion section). Overall, all four of the chemical kinetic models considered here do a good job of predicting the general trends in CH mole fraction for these four flames. CH radicals are found in a narrow region above the burner with peak mole fractions on the order of 2×10^{-5}, or 20 ppm. The largest discrepancy between the models and data is found for the height above burner in the richest flame investigated, $\phi = 1.6$.

Search for Vinyl Spectrum. Recently, Pibel et al.[53] detected the $A^2A''-X^2A'$ electronic transition of the vinyl radical (C_2H_3) by ringdown in the same spectral region as the CH $A^2\Delta-X^2\Pi$ transition. We searched for vinyl radical in the methane flames studied here with no success. There are no unassigned lines of greater than 50 ppm/pass signal intensity in the observed ringdown spectra. Within an order of magnitude, we estimate that the vinyl radical ringdown signal would be 0.5 ppm/pass, which would necessitate extensive signal averaging. Because the vinyl transitions are so broad, small fluctuations in the nonresonant background cavity ringdown signal also serve to obscure any potential vinyl radical signals. We also searched for vinyl radicals in a rich ($\phi = 1.9$) ethylene−oxygen−argon flame, which was expected to produce nearly an order of magnitude more vinyl radicals than the methane−oxygen−argon flames. Unfortunately, the amount of nonresonant cavity ringdown signal also increased significantly in the ethylene−oxygen−argon flame (presumably due to increased soot or soot precursor formation) and no vinyl radical signal was detected. Vinyl detection by cavity ringdown spectroscopy may be possible by probing transitions to the blue, where there is less interference from CH, and where vinyl has a larger absorption coefficient.

Discussion

Quantitative Profiling of CH Number Density. In order to compare our data with the model predictions, we must make an estimate of the experimental uncertainties. The Einstein *A* coefficients used to obtain the cross sections have associated error of ±3%.[35] The temperature measurements used to convert from absorption to mole fraction have uncertainties of ±75 K,[23] which lead to ±5% uncertainties in the mole fractions. From the pLIF images, we have shown that nonideal behavior of the burner can lead to errors in the path length of approximately ±10%. Combining these error sources leads to uncertainties of ±12%. As noted above, another source of error is the finite laser bandwidth. For our 0.02 cm^{-1} wide OPO and 0.20 cm^{-1} wide transitions, simulations of the ringdown decay show that this error is negligible. However, for our 0.15 cm^{-1} wide laser, a 100 ppm/pass background level and a strongly absorbing line

of 3000 ppm/pass, this error increases to a 25% underprediction when fitting the 90−10% portion of the ringdown. We note that this error is smaller for weaker absorbing lines that are closer to the background absorption level. For a 300 ppm/pass signal on a 100 ppm/pass background level, the error drops to 15% and for a 30 ppm/pass signal, the error is again negligible over reasonable fit limits for flame work. This reduction in error with decreasing signal is because the multiexponential behavior is pushed out later in time as the signal portion of the ringdown approaches the background level. Thus, in the case of weakly absorbing species, such as HCO and $^1CH_2$,[34] the laser bandwidth is less critical for obtaining accurate results. In this way, cavity ringdown spectroscopy is ironically more difficult with strongly absorbing species.

Because of our care in beam shaping and the use of a CCD camera in aligning the ringdown cavity, we observe sharp gradients in the mole fraction of CH versus the height above the burner. Our 72.5 cm long cavity with 6 m radius of curvature mirrors is predicted to have a beam waist diameter of 0.88 mm, with 0.91 mm diameter spots at the mirrors. The beam is thus nearly collimated in the cavity and has a predicted spatial resolution of <1 mm. Figure 1 shows that the injected beam is slightly smaller than the predicted dimensions, but evolves to these dimensions within a few microseconds. This cavity allows us sufficient spatial resolution to detect the important chemical changes in low-pressure flames as indicated by the excellent agreement of the model and data rise and fall slopes shown in Figure 8. It would be possible to enhance the spatial resolution by decreasing the radius of curvature of the mirrors and/or shortening the cavity. However, the ultimate gains are limited; a 72.5 cm long confocal cavity would give a 0.44 mm diameter beam waist. The cavity could be shortened to approximately 20 cm. A confocal cavity of this length would have a 0.23 mm beam waist, resulting in a 4-fold increase in spatial resolution from our current cavity.

The CCD camera system is particularly helpful in aligning the ringdown cavity for optimal spatial resolution (see Figure 1). The laser beam is initially aligned parallel to the burner surface by the use of pinholes mounted in the ringdown mirror mounts. As the mirrors are installed, the mirror mounts are slightly adjusted to align the laser back on itself through the pinholes in the two spatial filters. Fine-tuning of the cavity is accomplished by adjusting the exit ringdown mirror for maximum ringdown signal decay time. This procedure usually served to align the system so that two spots appear in the CCD image of the ringdown beam. These spots arise from transverse mode structure in the cavity. Small adjustments of the exit mirror serve to overlap the two spots, and thus align the ringdown cavity. It is noteworthy that the misalignment case shown in Figure 1 is for a minimal adjustment of the micrometer screw that controlled the exit mirror mount. The ringdown curves for the aligned and misaligned cases shown in Figure 1 look essentially identical on an oscilloscope trace. Since a slight misalignment of the ringdown cavity may degrade the spatial resolution of the technique, careful alignment is essential for optimal spatial resolution.

Cavity ringdown spectroscopy, as it is implemented in our laboratory, does not have sufficient spatial resolution to probe CH gradients in atmospheric pressure flames. Finer spatial resolution may be possible with a different cavity as described above. Using a similar optical setup to ours, Mercier et al.[28] have, however, used cavity ringdown spectroscopy of CH radicals to profile the direction transverse to the flame front in an atmospheric pressure diffusion flame on a Wollard−Parker slot burner. It is noteworthy that the shapes of their CH cavity ringdown profiles generally agree with those measured by LIF.

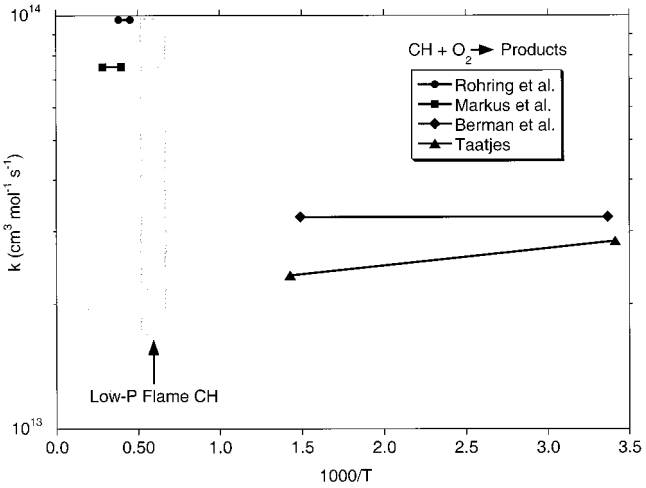

Figure 9. Arrhenius plot of the temperature-dependent literature values of the rate coefficient for the reaction CH + O_2. Experimental data are from shock tube experiments by Markus et al.,[33] and Rohrig et al,[32] and by flow-tube measurements of Berman et al.[54] and Taatjes.[52] The shaded region is applicable to the present low-pressure flame studies. GRI Mech 2.11[30] uses the 3.3×10^{13} cm^3 mol^{-1} s^{-1} rate coefficient of Berman et al.[54] without any temperature dependence. The modified GRI Mech 2.11 calculations shown in Figure 8 use the temperature coefficient of Rohrig et al.,[32] 9.68×10^{13} cm^3 mol^{-1} s^{-1}, also without temperature dependence.

CH Chemistry. Although all of the models shown in Figure 8 demonstrate good agreement with the data within the experimental uncertainties, it is worth considering whether some of the systematic discrepancies can be traced to inadequate chemistry in the models. In particular, we investigate the systematic over prediction of CH by GRI Mech 2.11. As highlighted by Woiki et al.,[31] CH is primarily consumed by reaction with NO. Thus, CH measurements in nitrogen-containing flames may mask other CH chemistry effects. In flames without nitrogen, such as those used in the present study, CH is lost primarily by fast reaction with O_2. Though this reaction is quite fast, reaction with NO is 4 times faster at temperatures below 1000 K.[52] Recent shock tube measurements[32,33] show that, for $T \geq 2000$ K, the rate coefficient for the CH + O_2 reaction should be 3 times larger than the low-temperature value used in GRI Mech 2.11. These measurements were not available when this mechanism was developed. Figure 9 shows an Arrhenius plot of the temperature dependence of the CH + O_2 rate coefficients for four experimental determinations as well as the temperature range appropriate for the present experiments. Since CH only exists in relatively high-temperature regions of the flame, the recent shock tube rates are more appropriate for flame modeling than those from the previous low-temperature data incorporated into GRI Mech 2.11.

We note that the authors of GRI Mech specifically advise against changing rates in the model since the published rate set is the result of a global optimization.[30] However, we feel that it is worth investigating the effect that this significant new CH + O_2 rate expression would have on the model, particularly since the CH targets used in the model all used nitrogen-doped flames that are insensitive to this rate. We do not suggest that such a modified model be used for quantitative prediction. When we carried out model calculations using GRI Mech 2.11 with the CH + O_2 rate coefficient of Rohrig et al.,[32] we found that the predicted CH mole fractions were 30% smaller than those for the GRI Mech 2.11 and that the CH mole fractions were,

indeed, closer to the CH mole fractions measured using cavity ringdown spectroscopy. GRI Mech 2.11 uses a temperature-independent value of 2.3×10^{13} cm^3 mol^{-1} s^{-1} for this rate coefficient. Experiments prior to the shock tube work show little temperature dependence for this reaction. The higher temperature experiments suggest that an additional reaction channel opens up in the temperature regime between the shock tube and flow tube experiments. There is a need for further experimental measurements of the CH + O_2 reaction rate in this intermediate flame temperature range to determine where this postulated new channel opens and what the products may be.

Late in the course of this work, the latest revision of the GRI Mech (version 3.0) became available.[4] This mechanism includes a refined CH + O_2 rate, as well as many other changes. Several changes affect the calculated CH concentration directly. The CH + H_2 rate has been modified in light of recent measurements, and the reaction CH + H_2 + M → CH_3 is now included. With these changes, the CH + H_2O rate has been lowered. For near-stoichiometric flames, this version produces better agreement with the data than GRI Mech 2.11, falling midway between the GRI Mech 2.11 curve and our modified GRI Mech 2.11 curve. At richer stoichiometries, GRI Mech 3.0 shows a higher peak CH concentration than that observed in the data. The Prada−Miller model[44] also shows good agreement with the data for near-stoichiometric flames, but then demonstrates a rapid decrease in CH concentration at higher values of ϕ, which is not evident in the data. None of the models show good agreement of the position of the CH concentration maximum or the downstream slope in the $\phi = 1.6$ flame. Since the 1.5−2.0 mm errors are beyond the experimental uncertainty, this discrepancy is most likely due to inaccuracies in the model. The leading candidate to explain this discrepancy is the onset of molecular weight growth processes leading to the formation of larger hydrocarbon products, which are not included in these models.

Detection Limits and Comparison with Other Methods. The detection limit for the present experiment, 3×10^9 cm^{-3}, is at least a factor of 5 better than that shown by groups using the $C^2\Sigma^+-X^2\Pi$ transition for ringdown.[27,28] The primary reason for this is the present availability of higher reflectivity mirrors at 430 nm ($R = 99.995+\%$ for our mirrors) than at 315 nm ($R = 99.6\%$ for Mercier et al.,[28] 99.75% for Derzy et al.[27]). Both the $C^2\Sigma^+-X^2\Pi$ and $A^2\Delta-X^2\Pi$ electronic transitions have been used quantitatively to measure CH radical concentrations at detection limits suitable for flame studies, and the choice of transition used to monitor CH may depend on factors such as the availability of light sources and ringdown mirrors. The $C^2\Sigma^+-X^2\Pi$ transition has the added feature (and complexity) of overlapping the OH $A^2\Delta-X^2\Pi$ transition. Since the $C^2\Sigma^+-X^2\Pi$ transition is more predissociated, the $B^2\Sigma^--X^2\Pi$ and $A^2\Delta-X^2\Pi$ transitions are more suitable for LIF. As direct absorption measurements may be used simultaneously with pLIF to place limits on the absolute concentrations, one may find that the primary utility of CH CRD is in providing quantitative limits for CH pLIF measurements. Though a published report has not appeared as of this writing, we have confidence that ringdown spectroscopy would also work on the CH $B^2\Sigma^--X^2\Pi$ transition near 385 nm. One might wish to probe the $B^2\Sigma^-$−$X^2\Pi$ transition as a complement to pLIF studies, because excitation of the $B^2\Sigma^--X^2\Pi$ transition with detection of the $A^2\Delta-X^2\Pi$ transition is optimal for pLIF studies.

Quantitative CH measurements, one of the main motivations for this work, still rely on an independent measure of the temperature. To convert the signal from any molecular spectroscopic technique, which gives the number density in a specific quantum state, to a total number density requires a temperature to account for the partitioning of molecules into the available energy levels. Though, in principle, CH cavity ringdown may be used to measure temperatures, it is in practice often better to employ a separate measure of temperature. For the lowest concentrations, with S/N ratios near detection limits, the temperatures calculated will have large uncertainties. This problem is ubiquitous for any spectroscopic technique. Cavity ringdown spectroscopy has the advantage over LIF, the other technique used in quantitative CH measurements, in that corrections for quenching are not needed. Quenching corrections add the additional complexity of a need to measure, or at least model the major species concentrations, or to accurately measure fluorescence lifetimes. Furthermore, cavity ringdown does not require the calibration of detection system efficiency, which is often a nontrivial part of quantitative LIF work.

In that it is a null-background technique, LIF has a detection sensitivity advantage over cavity ringdown spectroscopy in situations with low source emission. For CH in a low-emission plasma, Doerk et al.[17] report an LIF detection limit of 10^8 cm^{-3}, or 4×10^6 molecules/quantum state, in their probe volume. In this case, LIF is an order of magnitude more sensitive than cavity ringdown. For a high-emission plasma, however, Doerk et al.[17] report a LIF detection limit of 4×10^9 cm^{-3}, which is essentially the same sensitivity as they find for resonance-enhanced coherent anti-Stokes Raman spectroscopy (RECARS) in that environment. Cavity ringdown spectroscopy using the $A^2\Delta-X^2\Pi$ transition, with a 3×10^9 cm^{-3} detection limit in a low-pressure flame, is competitive with these techniques in a wide variety of environments.

For situations where source emission might hinder LIF or cavity ringdown detection, Williams et al.[11] suggest that degenerate four-wave mixing (DFWM) is an appropriate technique for measuring quantitative CH radical densities. In an atmospheric pressure oxyacetylene flame, they estimate a detection limit of 4×10^{11} cm^{-3} or 4×10^9 cm^{-3}/quantum state with DFWM having comparable sensitivity to LIF for their conditions. For the less-hostile environment considered in the present work, the cavity ringdown detection limit is 2 orders of magnitude more sensitive. DFWM, CARS, and TC-RFWM (two-color−resonant four-wave mixing) each have the disadvantage, however, that the signal is quadratically dependent on the density of the species being probed. An advantage of these nonlinear methods is that the signal comes out as a coherent beam of light, making it is easier to discriminate against background emission. Lee and co-workers[13−15] have taken advantage of the double-resonance feature of TC-RFWM in detecting new transitions in the CH $B^2\Sigma^--X^2\Pi$, $C^2\Sigma^+-X^2\Pi$, and $D^2\Pi-X^2\Pi$, systems.

Summary and Conclusion

We measure cavity ringdown spectra of the $A^2\Delta-X^2\Pi$ transition of the CH radical in a series of rich low-pressure methane−oxygen−argon flames and demonstrate that the technique is sensitive, quantitative, and straightforward in its implementation and interpretation. As a line-of-sight technique, it complements imaging techniques, such as planar laser-induced fluorescence. Our results generally agree with chemical kinetic models for methane oxidation that have appeared in the literature, but suggest some refinements are necessary. Additional examination of the CH + O_2 reaction rate as a function of temperature is advised. Our results are consistent with those of Derzy et al.[27] using the $C^2\Sigma^+-X^2\Pi$ transition for stoichio-

metric, low-pressure flames which include nitrogen. Our results for rich flames, as with earlier experiments for singlet methylene, suggest that flame chemical kinetic models need to be adjusted to account for flame chemistry for stoichiometries richer than $\phi = 1.5$.

Acknowledgment. This work is supported by the U.S. Department of Energy, Office of Basic Energy Sciences, Chemical Sciences Division. The authors thank David Crosley, Jay Jeffries, Jorge Luque, and Greg Smith of SRI International for helpful discussions. At the Combustion Research Facility, Sandia National Laboratories, Phil Paul provided stimulating conversations, and Ed Bochenski supplied expert technical assistance. J.W.T. thanks the President and Trustees of Williams College for the sabbatical leave that enabled him to visit Sandia.

References and Notes

(1) Miller, J. A.; Bowman, C. T. *Prog. Energy Combust. Sci.* **1989**, *15*, 287−338.
(2) Raiche, G. A.; Jeffries, J. B. *Appl. Opt.* **1993**, *28*, 4629−4635.
(3) Najm, H. N.; Paul, P. H.; Mueller, C. J.; Wyckoff, P. S. *Combust. Flame* **1998**, *113*, 312−332.
(4) Smith, G. P.; Golden, D. M.; Frenklach, M.; Moriarty, N. W.; Eiteneer, B.; Goldenberg, M.; Bowman, C. T.; Hanson, R.; Song, S.; W. C. Gardiner, J.; Lissianski, V.; Qin, Z. *Methane Combustion Kinetics Mechanism*, Version 3.0; sponsored by the Gas Research Institute, available at http://www.me.berkeley.edu/gri-mech/:.
(5) Najm, H. N.; Knio, O. M.; Paul, P. H.; Wyckoff, P. S. *Comb. Sci. Technol.* **1998**, *140*, 369.
(6) Paul, P. H.; Dec, J. E. *Opt. Lett.* **1994**, *19*, 998−1000.
(7) Bernath, P. F.; Brazier, C. R.; Olsen, T.; Hailey, R.; Fernando, W. T. M.; Woods, C.; Hardwick, J. L. *J. Mol. Spectrosc.* **1991**, *147*, 16−26.
(8) Luque, J.; Crosley, D. R. *Appl. Phys. B* **1996**, *63*, 91−98.
(9) Salmon, J. T.; Laurendeau, N. M. *Appl. Opt.* **1985**, *24*, 65−73.
(10) Renfro, M. W.; Klassen, M. S.; King, G. B.; Laurendeau, N. M. *Opt. Lett.* **1997**, *22*, 175−177.
(11) Williams, S.; Green, D. S.; Sethuraman, S.; Zare, R. N. *J. Am. Chem. Soc.* **1992**, *114*, 9122.
(12) Green, D. S.; Owano, T. C.; Williams, S.; Goodwin, D. G.; Zare, R. N.; Kruger, C. H. *Science* **1993**, *259*, 1726−1729.
(13) Kumar, A.; Hsiao, C. C.; Hung, W. C.; Lee, Y. P. *J. Chem. Phys.* **1998**, *109*, 3824−3830.
(14) Li, X.; Kumar, A.; Hsiao, C.-C.; Lee, Y.-P. *J. Phys. Chem.* **1999**, *103*, 6162−6166.
(15) Li, X.; Lee, Y.-P. *J. Chem. Phys.* **1999**, *111*, 4942−4947.
(16) Peterson, K. A.; Oh, D. B. *Opt. Lett.* **1999**, *24*, 667−669.
(17) Doerk, T.; Hertl, M.; Pfelzer, B.; Hadrich, S.; Jauernik, P.; Uhlenbusch, J. *Appl. Phys. B* **1997**, *64*, 111.
(18) O'Keefe, A.; Deacon, D. A. G. *Rev. Sci. Instrum.* **1988**, *59*, 2544−2551.
(19) Scherer, J. J.; Paul, J. B.; O'Keefe, A.; Saykally, R. J. *Chem. Rev.* **1998**, *97*, 25−51.
(20) *Cavity Ringdown Spectroscopy: An Ultratrace-Absorption Measurement Technique*; Busch, K. W., Busch, M. A., Eds.; American Chemical Society: Washington, DC, 1999; Vol. 720.
(21) Meijer, G.; Boogaarts, M. G. H.; Jongma, R. T.; Parker, D. H.; Wodtke, A. M. *Chem. Phys. Lett.* **1994**, *217*, 112−116.
(22) Lozovsky, V. A.; Derzy, I.; Cheskis, S. *Chem. Phys. Lett.* **1998**, *284*, 407−411.
(23) McIlroy, A. *Chem. Phys. Lett.* **1998**, *296*, 151−158.
(24) Scherer, J. J.; Aniolek, K. W.; Cernansky, N. P.; Rakestraw, D. J. *J. Chem. Phys.* **1997**, *107*, 6196−6203.
(25) Scherer, J. J.; Rakestraw, D. J. *Chem. Phys. Lett.* **1997**, *265*, 169−176.
(26) Thoman, J. W., Jr..; Tran, T.; Springfield, J.; Holdsworth, J.; Fernee, M.; Knight, A. E. W., private communication.
(27) Derzy, I.; Lozovsky, V. A.; Cheskis, S. *Chem. Phys. Lett.* **1999**, *306*, 319−324.
(28) Mercier, X.; Jamette, P.; Pauwels, J. F.; Desgroux, P. *Chem. Phys. Lett.* **1999**, *305*, 334−342.
(29) VanderWal, R. L.; Ticich, T. M. *Appl. Opt.* **1999**, *38*, 1444−1451.
(30) Smith, G. P.; Frenklach, M.; Wang, H.; Bowman, C. T.; Golden, D.; Gardiner, W.; Lissianski, V.; Serauskas, R. *Methane Combustion Kinetics Mechanism*, Version 2.11; sponsored by the Gas Research Institute, available at http://www.me.berkeley.edu/gri-mech/:.
(31) Woiki, D.; Votsmeier, M.; Davidson, D. F.; Hanson, R. K.; Bowman, C. T. *Combust. Flame* **1998**, *113*, 624−626.
(32) Rohrig, M.; Petersen, E. L.; Davidson, D. F.; Hanson, R. K.; Bowman, C. T. *Int. J. Chem. Kinet.* **1997**, *29*, 781−789.
(33) Markus, M. W.; Roth, P.; Just, T. *Int. J. Chem. Kinet.* **1996**, *28*, 171−179.
(34) McIlroy, A. *Isr. J. Chem.* **1999**, *39*, 55−62.
(35) Luque, J.; Crosley, D. R. *J. Chem. Phys.* **1996**, *104*, 3907−3913.
(36) Luque, J.; Crosley, D. R. *LIFBASE*: Database and Spectral Simulation Program (Version 1.5); SRI International, MP 99-009, 1999.
(37) Beenakker, C. I. M.; Verbeek, P. J. F.; Mohlmann, G. R.; Heer, F. J. d. *J. Quant. Spectrosc. Radiat. Transfer* **1975**, *15*, 333.
(38) Baas, R. Ch.; Beenakker, C. I. M. *Comput. Phys. Commun.* **1974**, *8*, 236−245.
(39) Garland, N. L.; Crosley, D. R. *J. Quant. Spectrosc. Radiat. Transfer* **1985**, *33*, 591−595.
(40) Kee, R. J.; Dixon-Lewis, G.; Warnatz, J.; Coltrin, M. E.; Miller, J. A. "A Fortran Computer Code Package for the Evaluation of Gas-Phase Multicomponent Transport Properties", Sandia National Laboratories, SAND86-8246.UC-32, 1986.
(41) Kee, R. J.; Grcar, J. F.; Smooke, M. D.; Miller, J. A. "A Fortran program for modeling steady laminar one-dimensional flames", Sandia National Laboratories, SAND85-8240.UC-4, 1987.
(42) Kee, R. J.; Rupley, F. M.; Miller, J. A. "Chemkin II: A Fortran Chemical Kinetics Package for the Analysis of Gas-Phase Chemical Kinetics", Sandia National Laboratories, SAND89-8009.UC-401, 1991.
(43) Kee, R. J.; Rupley, F. M.; Miller, J. A. "The Chemkin Thermodynamic Database", Sandia National Laboratories, SAND87-8251B.UC-4, 1991.
(44) Prada, L.; Miller, J. A. *Combust. Sci. Technol.* **1998**, *132*, 225−250.
(45) Gero, L. *Z. Phys.* **1941**, *118*, 27.
(46) Zachwieja, M. *J. Mol. Spectrosc.* **1997**, *182*, 18.
(47) *CRC Handbook of Chemistry and Physics*; 56th ed.; Weast, R. C., Ed.; CRC Press: Cleveland, OH, 1976.
(48) Sappey, A. D.; Hill, E. S.; Settersten, T.; Linne, M. A. *Opt. Lett.* **1998**, *23*, 954−956.
(49) Zalicki, P.; Zare, R. N. *J. Chem. Phys.* **1995**, *102*, 2708−2717.
(50) Romanini, D.; Lehmann, K. K. *J. Chem. Phys.* **1993**, *99*, 6287−6301.
(51) Hodges, J. T.; Looney, J. P.; Van Zee, R. D. *Appl. Opt.* **1996**, *35*, 4112−4116.
(52) Taatjes, C. A. *J. Phys. Chem.* **1996**, *100*, 17840−1784.
(53) Pibel, C. D.; McIlroy, A.; Taatjes, C. A.; Alfred, S.; Patrick, K.; Halpern, J. B. *J. Chem. Phys.* **1999**, *110*, 1841−1843.
(54) Berman, M. R.; Fleming, J. W.; B.Harvey, A.; Lin, M. C. "Temperature Dependence of CH Radical Reactions with O_2, NO, CO and CO_2"; Nineteenth Symposium (International) on Combustion, Pittsburgh, PA, 1982.